Geometrical dependence of molecular-frame photoelectron emission from H_2^+

R. Della Picca, P. D. Fainstein,* and M. L. Martiarena
Centro Atómico Bariloche, Comisión Nacional de Energía Atómica, Avda E. Bustillo 9500, 8400 Bariloche, Argentina

A. Dubois
Laboratoire de Chimie Physique-Matière et Rayonnement, Université Pierre et Marie Curie, 11 rue Pierre et Marie Curie, 75231 Paris Cedex 05, France

(Received 17 April 2006; revised manuscript received 26 May 2006; published 13 March 2007)

We study the photoemission spectra of the hydrogen molecular ion for various geometrical arrangements. For different angles between the internuclear axis and the polarization vector, we calculate the angular distribution and analyze the results in terms of the symmetries and partial-wave contributions to the spectra. Contrary to previous studies we find that the angular distribution is not aligned with the internuclear axis or the polarization vector. The alignment is determined by the coherent superposition of $\sigma \rightarrow \sigma$ and $\sigma \rightarrow \pi$ transition amplitudes and by the relative contributions from the different partial waves, strongly dependent on the photoelectron energy.

DOI: 10.1103/PhysRevA.75.032710 PACS number(s): 34.80.−i, 33.80.−b

I. INTRODUCTION

Angular distributions of electrons emitted in collisions between photons or charged particles with atoms or molecules provide detailed information about the collision dynamics [1]. For ion impact the required integration over the momentum transfer impedes the complete understanding of the process and photons are therefore the cleanest probe to study electron emission. For photon impact on atoms the process is strictly dipolar while for molecular targets high angular momentum partial waves can contribute to the cross sections. It is, however, possible to obtain, both theoretically and experimentally, the angular momentum components of the final electronic distributions, in energy or angle of emission [2,3]. These distributions depend on several parameters such as the internuclear distance, the electron energy, and, for linear polarization, the angle between the molecular axis and the polarization vector. In a recent experimental study of the photofragmentation of the deuterium molecule [4], the photoelectron angular distribution was measured for different orientations and internuclear distances of the target molecule. This experiment showed that the angular distribution is highly sensitive to these features and depends markedly on the target wave functions.

The theoretical description of photoelectron emission processes from molecules involves multicenter electronic states. The calculation of the continuum wave functions is significantly more difficult than that of the corresponding bound states. While the latter can be represented with very high accuracy using the Hartree-Fock or density-functional methods, stronger approximations must be employed to represent the continuum states. In most cases these are represented by a product of one-center wave functions so that they can be viewed as first-order perturbative approximations to the exact ones. The first study of the photoelectron *angular distribution* from diatomic molecules (H_2^+ and H_2) was performed by Walter and Briggs [5]. Their model was based on the approximate representation of both the initial ground state and final continuum states employing a simple linear combination of atomic orbitals (LCAO) and a product of two one-center wave functions (2C approximation), corresponding to the interaction between the emitted electron and each nucleus of the molecule, respectively. These authors showed that significant departures appeared with respect to previous results obtained employing plane waves to represent the final states [6]. The method of [5] allows us to obtain the transition amplitude in analytical form and is then useful for the computation of cross sections. Recently it has been employed to study photoionization, photorecombination, bremsstrahlung, and Compton ionization by monochromatic photon fields and by attosecond x-ray pulses [7,8].

Very recently, Rescigno *et al.* [9] and Della Picca *et al.* [10] (to be referred hereafter as paper I) performed exact calculations which showed significant departures from the results obtained with the perturbative approximation. To test without ambiguity the 2C approximation, Della Picca *et al.* [10] made the same calculation as Walter and Briggs [5] replacing their approximate final state by the exact wave function. These results were compared with exact calculations which were employed as benchmark. This detailed study showed that the 2C approximation failed to represent the angular distribution up to a few hundredths eV. Interestingly, Yudin *et al.* [7], however, found that the angular distributions calculated with the 2C approximation were in excellent agreement with the exact calculations for very large values of the internuclear distance ($R=8$ a.u.) and high photon energy ($\hbar\omega=100$ eV).

Della Picca *et al.* [10] and Yudin *et al.* [7] restricted their analysis to the case where the (linear) polarization vector and the molecular axis are either parallel or perpendicular. These geometries have the particular feature that, due to the symmetry of the problem, only $\sigma \rightarrow \sigma$ and $\sigma \rightarrow \pi$ transitions are allowed, respectively. These symmetries are broken for other relative orientations of these two vectors and the analysis of the angular distribution is thus more complicated. Rescigno

*Electronic address: pablof@cab.cnea.gov.ar

et al. [9] performed exact calculations for different orientations of the polarization vector ($\hat{\varepsilon}$) and the internuclear axis ($\hat{R}$) at 10 eV electron energy. Their results exhibit large departures with respect to the perturbative results. These authors noted that the angular distribution *appears* to be aligned with the electric field, contrary to the results from the 2C approximation which have predicted that the angular distribution is aligned in the direction of the internuclear axis.

The objective of the present work if therefore to study the alignment of the angular distributions as a function of the geometrical arrangement between the internuclear axis and the polarization vector. For that purpose we extend the analysis of Rescigno *et al.* [9] considering different angles between the two vectors, several electron energies, and different internuclear distances. Atomic units will be used except when otherwise stated.

II. THEORY

In this section we briefly review the method of calculation and the main results obtained in paper I. We assume that the nuclei remain fixed at the equilibrium internuclear distance ($R=2$ a.u. for H_2^+) and therefore neglect the vibrational and rotational motions of the molecule. The molecular and laboratory reference frames are defined as in Fig. 1 of [10].

The electronic transition matrix in the dipole approximation is given by

$$T_{fi}^{el} = \langle \psi^{(-)}(\mathbf{k}_e, \mathbf{r}) | \hat{\varepsilon} \cdot \boldsymbol{\nabla}_{\mathbf{r}} | \psi_i(\mathbf{r}) \rangle, \tag{1}$$

where $\mathbf{k}_e \equiv \{k_e, \theta_e, \phi_e\}$ is the ejected electron momentum in the molecular frame and $E_e = k_e^2/2$ is the corresponding photoelectron energy.

To obtain the initial ψ_i and final $\psi^{(-)}(\mathbf{k}_e, \mathbf{r})$ states we solve numerically the electronic Schrödinger equation, with the appropriate asymptotic conditions, using well established computational methods [11–13].

With the initial and final wave functions we calculate numerically the transition matrix (1) from which we obtain the differential cross section for the fixed in-space molecule as a function of the photoelectron energy and angle:

$$\frac{d\sigma}{d\hat{R}\, d\hat{k}_e} = \frac{(2\pi)^2 \alpha}{\omega} |T_{fi}^{el}|^2, \tag{2}$$

where $\hat{k}_e$ is the direction of the emitted photoelectron in the molecular reference frame, $\hat{R} \equiv \{\Theta_R, \Phi_R\}$ is the orientation of the molecule with respect to the laboratory reference frame (defined by the radiation field), and α is the fine structure constant. The differential cross section can be integrated over the orientation of the molecule and the emission angle of the photoelectron to get the total cross section. We calculate these values to check with the ones obtained previously with the similar methods by Richards and Larkins [14]. We note that these results are practically indistinguishable from those obtained with the analytical Guillemin-Zener (GZ) wave function [25] for the initial state used in paper I. This validates the use of the GZ wave function in analytical calculations, as opposed to the simple LCAO model state which has been shown to fail in many cases (see [15] and references therein).

The transition matrix (1) can be expressed as

$$T_{fi}^{el} = m_\sigma \cos \Theta_R + m_\pi \sin \Theta_R, \tag{3}$$

where m_σ and m_π are body fixed $\sigma \rightarrow \sigma$ and $\sigma \rightarrow \pi$ electronic dipole transition elements, respectively. m_σ and m_π can be written as a series of odd associated Legendre functions (partial waves):

$$m_\sigma = C \sum_{n=0}^{\infty} f_{2n+1}^{\sigma} P_{2n+1}^{0}(\cos \theta_e), \tag{4}$$

$$m_\pi = -C \cos \phi_e \sum_{n=0}^{\infty} f_{2n}^{\pi} P_{2n+1}^{1}(\cos \theta_e), \tag{5}$$

where C is a constant.

III. RESULTS AND DISCUSSIONS

A. Angular distributions: Geometrical dependence

Equation (3) shows that, when the molecular axis and the polarization vector are in the same direction ($\Theta_R = 0$), only $\sigma \rightarrow \sigma$ transitions are allowed. On the contrary, when these vectors are at right angles, only $\sigma \rightarrow \pi$ transitions can occur. For other values of Θ_R it is straightforward to obtain from Eqs. (2) and (3) that the differential cross section is given by

$$\frac{d\sigma}{d\hat{R}\, d\hat{k}_e} = \frac{(2\pi)^2 \alpha}{\omega} [m_\sigma^2 \cos^2 \Theta_R + m_\pi^2 \sin^2 \Theta_R + 2\, \mathbf{Re}\{m_\sigma^* m_\pi\} \cos \Theta_R \sin \Theta_R]. \tag{6}$$

We see therefore that the differential cross section is thus given by the incoherent sum of $\sigma \rightarrow \sigma$ and $\sigma \rightarrow \pi$ cross sections, with weights $\cos^2 \Theta_R$ and $\sin^2 \Theta_R$, respectively, and an interference term. The differential cross section for any value of Θ_R is therefore determined by the corresponding values for parallel and perpendicular alignment of the internuclear axis and the polarization vector. As shown in paper I the coefficients f_{2n+1}^{σ} and f_{2n}^{π} in Eqs. (4) and (5) are strongly dependent on the photoelectron energy. The angular distribution for different angles between the molecular axis and the polarization vector (Θ_R) will therefore reflect the competition between the two different types of transitions and the dependence of the angular momentum components on the electron energy. This behavior will therefore determine if the angular distribution is aligned along the molecular axis, as predicted by the 2C approximation, or in any other particular direction. At low electron energy the $f\sigma$ and $p\pi$ partial waves give the main contribution to the $\sigma \rightarrow \sigma$ and $\sigma \rightarrow \pi$ transitions, respectively. As the electron energy increases many partial waves contribute and the angular distribution is determined by their coherent sum. We therefore choose for the present study four values: 10, 50, 150, and 250 eV and analyze the angular distributions in the molecular frame. As in paper I we consider for simplicity the co-planar geometry in which the photoelectron momenta, polarization and inter-

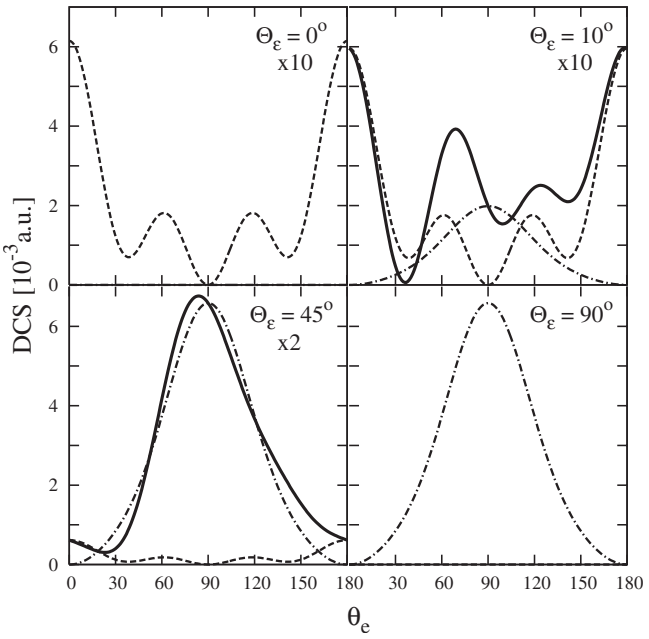

FIG. 1. H_2^+ molecular frame photoionization differential cross section for 10 eV electron energy and $\Theta_\varepsilon = 0°, 10°, 45°, 90°$.

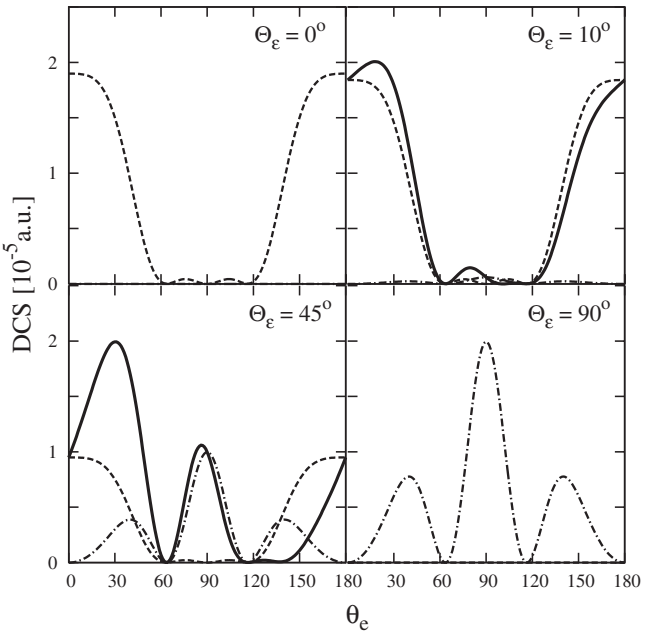

FIG. 3. Same as Fig. 2 for 150 eV electron energy.

nuclear vectors are all in the same plane. The angle Θ_R was defined in paper I as the angle between the polarization vector and the internuclear axis. Here, as we analyze the results in the molecular frame, we introduce the angle Θ_ε $(=-\Theta_R)$ as the angle of the polarization vector in the molecular frame. In the following, for each value of Θ_ε we calculate the angular distribution as a function of θ_e.

In Figs. 1–4 we plot the full result, in the solid line, and the contributions from the $\sigma \rightarrow \sigma$ and $\sigma \rightarrow \pi$ transitions as the dashed and dot-dashed lines, respectively, for the four photoelectron energies indicated above. In some plots the results have been multiplied by the indicated factors to put them all on the same scale. In Fig. 5 all these results are summed up as polar plots. From these figures one can identify, at each angle Θ_ε, the weighted contribution from the two types of transitions. As the full transition amplitude is given by the coherent sum of electronic dipole transition elements, m_σ and m_π, there are of course interference effects, as can be readily recognized by the asymmetry of the peaks at 60° and 120° for $\Theta_\varepsilon = 10°$ in Fig. 1. In the electron energy range considered here the angular distribution for parallel alignment $(\Theta_\varepsilon = 0°)$ has distinct $f\sigma$, $p\sigma$, and $h\sigma$ symmetries as the electron energy increases. For perpendicular alignment $(\Theta_\varepsilon$

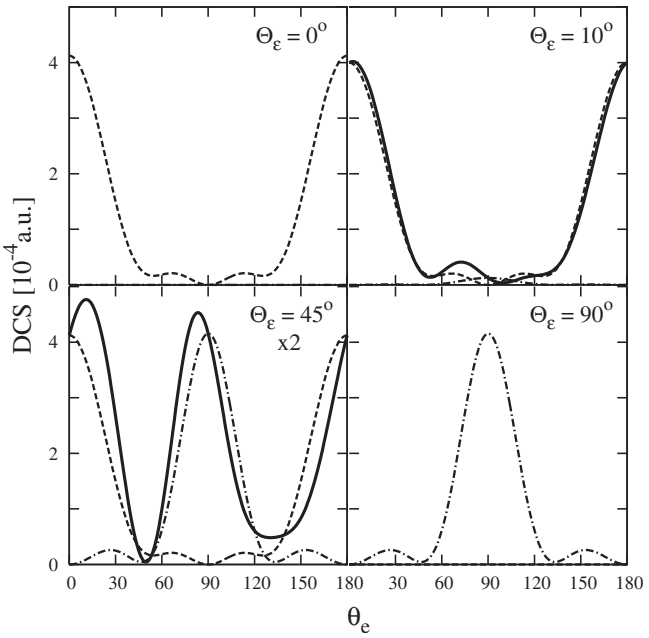

FIG. 2. Same as Fig. 1 for 50 eV electron energy.

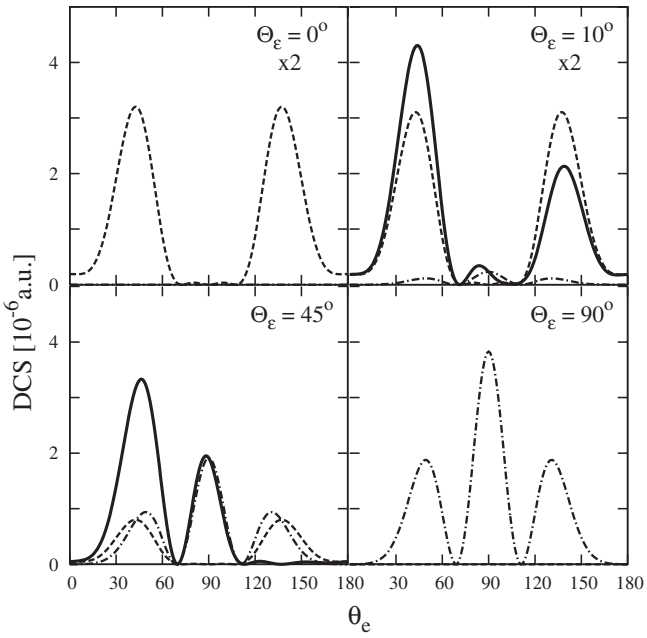

FIG. 4. Same as Fig. 2 for 250 eV electron energy.

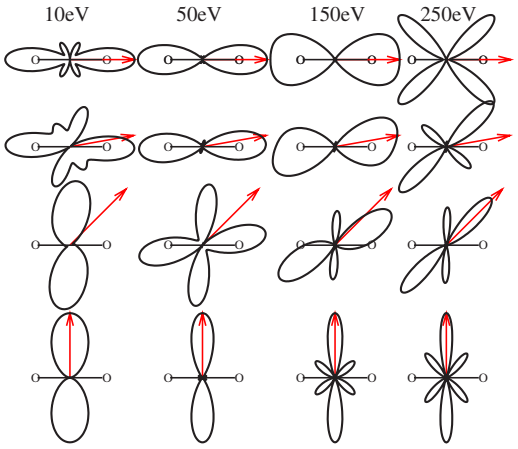

FIG. 5. (Color online) The results from Figs. 1–4 in polar representation.

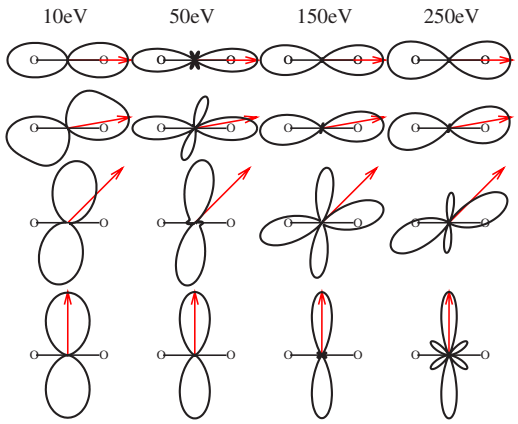

FIG. 6. (Color online) H_2^+ ($R=1.4$ a.u.) molecular frame photoionization differential cross section for 10, 50, 150, and 250 eV electron energy for $\Theta_\varepsilon=0°, 10°, 45°, 90°$.

$=90°$) the angular distribution has dominant $p\pi$ and $f\pi$ symmetries at low and high energies, respectively. These partial waves always display a maximum in the direction perpendicular to the molecular axis, i.e., in the direction of the polarization vector. The resulting angular distribution for other values of Θ_ε have therefore a component in the direction of the molecular axis, arising from the $\sigma \rightarrow \sigma$ transitions, and a component in the perpendicular direction, arising from $\sigma \rightarrow \pi$ transitions. Therefore, except for the case of $\Theta_\varepsilon=0°$ and at very small angles, the angular distribution shows no preference for emission in the direction of the molecular axis as predicted by the 2C approximation. By the same token, there is no preference for alignment by the electric field. As an example we consider the $\Theta_\varepsilon=45°$ case. At 10 and 50 eV the $\sigma \rightarrow \pi$ contribution is much larger than the $\sigma \rightarrow \sigma$ contribution, and therefore the angular distribution is oriented in the direction perpendicular to the internuclear axis. The small departure from this direction, to lower angles, is due to the interference between the two transition amplitudes which is not negligible. At 150 and 250 eV, both transition amplitudes give contributions of the same order. This gives rise to a lobe in the angular distribution close to $\theta_e=45°$, i.e., in the direction of the polarization vector. We cannot conclude, however, that these are general features. Each case requires a detailed analysis of the partial-wave contributions to the transition amplitudes.

Very recently, Selstø *et al.* [16] studied the geometrical dependence of the angular distributions but in the context of multiphoton ionization of H_2^+ by high intensity, high-frequency, ultrashort laser pulses. Interestingly, the results presented here in Fig. 2 and in the second column of Fig. 5 can be compared with the results shown in the second row of Figs. 5 and 6 of their work. Independently of the photon field characteristics we observe striking similarities. For $\Theta_\varepsilon=0°$ both results show the $\sigma \rightarrow \sigma$ symmetry with contributions from $p\sigma$ and $f\sigma$ partial waves, the latter giving rise to the two smaller maxima (note that in [16] the angles are taken with respect to the polarization vector). For $\Theta_\varepsilon=90°$ both results show the same $\sigma \rightarrow \pi$ symmetry with dominant contribution from the $p\pi$ partial wave. For $\Theta_\varepsilon=45°$ the angular distribution is similar although the relative values of the peaks are different. It is therefore the two-center geometry of the molecular target which determines the main features, such as the interferences, in the photoelectron angular distribution.

B. Angular distributions: Dependence on the internuclear distance

Paper I displayed for one photoelectron energy the dependence of the angular distribution upon the target internuclear distance. By varying this parameter comparisons with experimental results for photoionization of H_2 [17,18] and of the N_2 K-shell [19,20] (cf. also [21,22]) were also presented. As the internuclear distances for N_2 and H_2^+ are comparable, there are great similarities in the angular distribution of the photoelectrons emitted from these targets. H_2 is, however, quite different since the internuclear distance is much shorter. We have therefore carried out new calculations for $R=1.4$ a.u. and various polarization directions. Note that in this section our purpose is not to present accurate cross sections for H_2, which would require a complete two-electron treatment [23,24], but to compare only *qualitatively* the angular distributions for different values of R.

Figure 6 displays the angular distributions for $R=1.4$ a.u. and different angles between the molecular axis and the polarization vector. These results are quite different from the ones plotted in Fig. 5 ($R=2$ a.u.). The angular distributions for parallel alignment show a $p\sigma$ character except in a well defined range (around 50 eV) where the contribution from this partial wave goes through a minimum (a Cooper-like minimum) in favor of the $f\sigma$ ones, cf. [24]. For perpendicular alignment ($\hat{R} \perp \hat{\varepsilon}$) the angular distribution has a distinct $p\pi$ character up to 150-eV energy beyond which the contribution from the $f\pi$ partial waves starts to be important.

From the comparison between our results at 50 eV and Fig. 7 of [24], it appears that our one-electron calculations show the same qualitative behavior as the full two-electron calculations, except for parallel alignment where the latter shows additional structures. Most notably it is shown that for

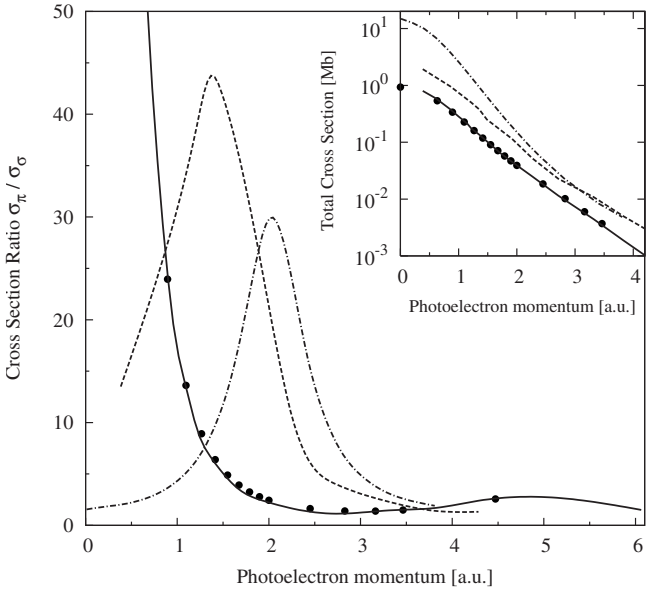

FIG. 7. Ratio σ_π/σ_σ between the $\sigma \rightarrow \sigma$ (σ_σ) and $\sigma \rightarrow \pi$ (σ_π) contributions to the total cross section. Inset: total cross section $\sigma = \sigma_\sigma + \sigma_\pi$. Theory, solid line, present results for H_2^+; (•), results for H_2^+ from [14]; dashed line, present results for H_2^+ with $R = 1.4$ a.u. (the total cross section is multiplied by 2); dot-dashed line, results for H_2 from [24].

$\Theta_\varepsilon = 45°$ the angular distribution does not follow the polarization direction. This feature stems from the fact that the contribution from the $p\pi$ partial wave is larger than the corresponding one from the $p\sigma$ partial wave.

From the above analysis our present one-electron calculations seem to reproduce qualitatively the results from more involved methods which account for the two electrons of the hydrogen molecule. It is therefore interesting to pursue this investigation to analyze if these similarities are just fortuitous or arise because both models take into account the same physics. To this end we analyze the $\sigma \rightarrow \sigma$ (σ_σ) and $\sigma \rightarrow \pi$ (σ_π) contributions to the total cross sections by plotting the ratio σ_π/σ_σ in Fig. 7. The ratio is computed for two internuclear distances, $R = 1.4$ and 2 a.u., and compared with the calculations by Richards and Larkins [14] and Semenov and Cherepkov [24], respectively, which are taken as benchmarks. For H_2^+ ($R = 2$ a.u.) the ratio is a monotonic decreasing function in excellent agreement with the results from [14], as the total cross sections $\sigma = \sigma_\sigma + \sigma_\pi$ shown in the inset.

On the contrary, for $R = 1.4$ a.u. the ratio shows a maximum, in qualitative agreement with the results for H_2 [24]. This peak arises from a dip in the $p\sigma$ contribution to σ_σ, steaming from the Cooper-like minimum. The inset also shows the total cross sections for that internuclear distance. Both calculations converge to the same values for energies above about 100 eV ($k_e > 3$ a.u.). At lower photoelectron energies a large disagreement shows up, demonstrating the importance of a correct treatment of the interelectronic repulsion in that range. However, both the one- and two-electron calculations provide similar explanations for the behavior of differential and total cross sections, although the former cannot reproduce exactly the position of the maximum and the absolute values of the different contributions.

Comparing the angular distributions shown in Figs. 5 and 6 one can find interesting similarities at high photoelectron energy. For example, the angular distributions for $R = 2$ a.u. at 50 eV are indeed similar to the ones for $R = 1.4$ a.u. at 150 eV. The same feature can be seen comparing the results at 150 and 250 eV, respectively. To explain this we note that the coefficients f_{2n+1}^{σ} and f_{2n}^{π} in Eqs. (4) and (5) depend on k_e, R, and the quantity $(k_e R/2)$. Taking only into account this last factor, a simple scaling relation can be derived, $E_e(R = 1.4) \simeq 2 \times E_e(R = 2)$, to predict the values of the photoelectron energies E_e which would present similar angular distributions for the two internuclear distances. This scaling is verified by the data displayed in Figs. 5 and 6, only at high photoelectron energy. For the lowest values the angular distributions do not follow the scaling law showing that the coefficients f_{2n+1}^{σ} and f_{2n}^{π} have a more complex dependence on k_e and R.

IV. CONCLUSIONS

We have studied the molecular frame angular distributions of photoelectrons emitted from H_2^+ as a function of internuclear distance, electron energy, and angle between the molecular axis and the polarization vector. The observed patterns stem from the coherent superposition of $\sigma \rightarrow \sigma$ and $\sigma \rightarrow \pi$ distributions corresponding to parallel and perpendicular alignment of the two vectors, respectively. The $\sigma \rightarrow \sigma$ and $\sigma \rightarrow \pi$ contributions are mainly oriented parallel and perpendicular to the molecular axis. The *apparent* alignment of the angular distribution with the electric field at 10 eV arises, as indicated by Rescigno *et al.* [9], from the much larger contribution of the $\sigma \rightarrow \pi$ cross section. For different photoelectron energy the alignment of the angular distribution depends therefore on the relative weight and the interference between both amplitudes. As a consequence the angular distributions do not show a general propensity for alignment with the molecular axis or the polarization vector. By the same token the alignment depends quite strongly on the internuclear distance.

ACKNOWLEDGMENT

P.D.F. and M.L.M. acknowledge support from CONICET. Laboratoire de Chimie Physique-Matière et Rayonnement is Unité Mixte de Recherche du CNRS (UMR 7614).

[1] *Many-Particle Quantum Dynamics in Atomic and Molecular Fragmentation*, edited by J. Ullrich and V. P. Shevelko (Springer-Verlag, Berlin, 2003).
[2] D. Dill, J. Chem. Phys. **65**, 1130 (1976).
[3] M. Lebech, J. C. Houver, D. Dowek, and R. R. Lucchese, Phys. Rev. Lett. **96**, 073001 (2006).
[4] T. Weber, A. O. Czasch, O. Jagutzki, A. K. Müller, V. Mergel, A. Kheifets, E. Rotenberg, G. Melgs, M. H. Prior, S. Daveau, A. Landers, C. L. Cocke, T. Osipov, R. Díz Muiño, H. Schmidt-Böcking, and R. Dörner, Nature (London) **431**, 437 (2004).
[5] M. Walter and J. Briggs, J. Phys. B **32**, 2487 (1999).
[6] H. D. Cohen and U. Fano, Phys. Rev. **150**, 30 (1966).
[7] G. L. Yudin, S. Chelkowski, and A. D. Bandrauk, J. Phys. B **39**, L17 (2006).
[8] G. L. Yudin, S. Patchkovskii, and A. D. Bandrauk, J. Phys. B **39**, 1537 (2006).
[9] T. N. Rescigno, D. A. Horner, F. L. Yip, and C. W. McCurdy, Phys. Rev. A **72**, 052709 (2005).
[10] R. Della Picca, P. D. Fainstein, M. L. Martiarena, and A. Dubois, J. Phys. B **39**, 473 (2006).
[11] G. Hadinger, M. Aubert-Frécon, and G. Hadinger, J. Phys. B **22**, 697 (1989).
[12] L. I. Ponomarev and L. N. Somov, J. Comput. Phys. **20**, 183 (1976).
[13] J. Rankin and W. R. Thorson, J. Comput. Phys. **32**, 437 (1979).
[14] J. A. Richards and F. P. Larkins, J. Phys. B **19**, 1945 (1986).
[15] O. A. Fojón, A. Palacios, J. Fernández, R. D. Rivarola, and F. Martín, Phys. Lett. A **350**, 371 (2006).
[16] S. Selstø, J. F. McCann, M. Førre, J. P. Hansen, and L. B. Madsen, Phys. Rev. A **73**, 033407 (2006).
[17] Y. Hikosaka and J. H. D. Eland, Chem. Phys. **277**, 53 (2002).
[18] A. Lafosse, M. Lebech, J. C. Brenot, P. M. Guyon, L. Spielberger, O. Jagutzki, J. C. Houver, and D. Dowek, J. Phys. B **36**, 4683 (2003).
[19] E. Shigemasa, J. Adachi, M. Oura, and A. Yagishita, Phys. Rev. Lett. **74**, 359 (1995).
[20] A. Yagishita, in *Photonic, Electronic and Atomic Collisions*, edited by F. Aumayr and H. Winter (World Scientific, Singapore, 1998), p. 149.
[21] R. Díez Muiño, D. Rolles, F. J. García deAbajo, C. S. Fadley, and M. A. Van Hove, J. Phys. B **35**, L359 (2002).
[22] T. Jahnke *et al.*, Phys. Rev. Lett. **88**, 073002 (2002).
[23] H. Bachau, E. Cormier, P. Decleva, J. E. Hansen, and F. Martín, Rep. Prog. Phys. **64**, 1815 (2001).
[24] S. K. Semenov and N. A. Cherepkov, J. Phys. B **36**, 1409 (2003).
[25] S. Kim, T. Y. Chang, and J. O. Hirschfelder, J. Chem. Phys. **43**, 1092 (1965).